Geophysical Research Letters

RESEARCH LETTER
10.1029/2024GL109364

Advantages of Inter-Calibration for Geostationary Satellite Sensors Onboard Twin Satellites

Yeeun Lee[1], Myoung-Hwan Ahn[1], Mina Kang[1], Mijin Eo[1], Dohyeong Kim[2], and Kyung-Jung Moon[3]

[1]Department of Climate and Energy Systems Engineering, Ewha Womans University, Seoul, South Korea, [2]National Meteorological Satellite Center, Korea Meteorological Administration, Jincheon, South Korea, [3]National Institute of Environmental Research, Incheon, South Korea

Key Points:

- Inter-calibration based on ray-matching between geostationary satellite sensors onboard twin satellites
- Implementation of collocation process in the visible wavelengths and the application of weighted statistics for ensuring collocation stability
- The novel advantages of the GEO-GEO inter-calibration approach for future applications

Supporting Information:

Supporting Information may be found in the online version of this article.

Correspondence to:

M.-H. Ahn,
terryahn65@ewha.ac.kr

Citation:

Lee, Y., Ahn, M.-H., Kang, M., Eo, M., Kim, D., & Moon, K.-J. (2024). Advantages of inter-calibration for geostationary satellite sensors onboard twin satellites. *Geophysical Research Letters*, *51*, e2024GL109364. https://doi.org/10.1029/2024GL109364

Received 21 MAR 2024
Accepted 3 JUL 2024

Author Contributions:

Conceptualization: Yeeun Lee, Myoung-Hwan Ahn
Data curation: Yeeun Lee, Mina Kang, Mijin Eo, Kyung-Jung Moon
Formal analysis: Yeeun Lee
Funding acquisition: Myoung-Hwan Ahn
Investigation: Yeeun Lee, Myoung-Hwan Ahn, Dohyeong Kim
Methodology: Yeeun Lee, Mina Kang, Mijin Eo
Project administration: Myoung-Hwan Ahn
Resources: Kyung-Jung Moon
Software: Yeeun Lee
Supervision: Myoung-Hwan Ahn
Validation: Yeeun Lee, Myoung-Hwan Ahn

© 2024. The Author(s).
This is an open access article under the terms of the Creative Commons Attribution-NonCommercial-NoDerivs License, which permits use and distribution in any medium, provided the original work is properly cited, the use is non-commercial and no modifications or adaptations are made.

Abstract To address the increasing demand for diurnal information on trace gases and aerosols, a series of geostationary (GEO) satellite programs called GEO-constellation have been initiated, with the launch of the Geostationary Environment Monitoring Spectrometer (GEMS) onboard Geostationary Korea Multi-Purpose Satellite 2B (GK2B). To assess the sensor performance of GEMS in orbit, the current work suggests employing an inter-calibration methodology involving the Advanced Meteorological Imager (AMI) aboard its twin satellite, GK2A. Twin satellites have a significant advantage in obtaining collocation data sets across diverse spatiotemporal, angular, and atmospheric conditions, enabling rigorous collocation criteria effectively reducing mismatch uncertainty. The results present robust correlation coefficients over 0.99, revealing the current calibration characteristics of the sensors. This research emphasizes the advantages of the GEO-GEO inter-calibration, particularly the capability of analyzing spatial and temporal dependencies. These findings confirm the mutual benefit of utilizing the sensors in similar configurations, highlighting their importance for future satellite monitoring endeavors.

Plain Language Summary Understanding diurnal changes in air pollutants is crucial for grasping how these substances move and disperse in the air, thereby aiding efforts to reduce pollution. In this regard, satellites have a distinct advantage in observation owing to their wide spatial coverage at regular time intervals. GEMS is one of the geostationary sensors providing such information for the Asia-Pacific region, nearly 7–8 times a day. To evaluate the reliability of GEMS, this study proposes an inter-calibration method by comparing GEMS observations with those of AMI aboard GK2A. These satellites have a unique advantage as they fly close to each other, observing the Earth with matched optical viewing paths. Scenes simultaneously observed by AMI and GEMS exhibit strong agreement, thus revealing the inherent observation characteristics of each sensor. These findings confirm the mutual benefit of utilizing the sensors in similar configurations for satellite monitoring during the operation.

1. Introduction

A global network of geostationary (GEO) satellites for air quality monitoring is to be established soon, including the Geostationary Environment Monitoring Spectrometer (GEMS), Tropospheric Emissions: Monitoring of Pollution (TEMPO) and the Ultraviolet Visible Near-infrared (UVN) instrument over East Asia, Northern America, and Europe, respectively. These GEO satellite sensors measure specific areas multiple times a day, which gives a significant advantage in providing diurnal information on trace gases and aerosol properties (J. Kim et al., 2020; Zoogman et al., 2017). Observations obtained from the GEO constellation will be crucial for monitoring the long-range transport of air pollutants as well as its diurnal variation. However, effective utilization of the measurements for global monitoring relies on ensuring consistency across sensors with varying designs, specifications, and calibration processes. This underscores the need for implementing measures to monitor measurement quality throughout their operational periods.

In this regard, inter-calibration has been an effective measure for post launch calibration (Chander et al., 2013). Especially for GEO sensors, ray-matching with low Earth orbit (LEO) satellite sensors has been widely applied, considering that LEO sensors cover different field of regards (FOR) of various GEO imagers (Doelling et al., 2016; Jiang et al., 2009; Minnis et al., 2002a, 2002b). Ray-matching between GEO-GEO sensors, however, has not been fully investigated as the FORs of GEO sensors cover distinct regions, like in the case of GEMS and TEMPO. Consequently, this technique has primarily been applied to infrared sensors on the same platform (Di

19448007, 2024, 14, Downloaded from https://agupubs.onlinelibrary.wiley.com/doi/10.1029/2024GL109364 by Ewha Womans University Library, Wiley Online Library on [30/10/2024]. See the Terms and Conditions (https://onlinelibrary.wiley.com/terms-and-conditions) on Wiley Online Library for rules of use; OA articles are governed by the applicable Creative Commons License

Visualization: Yeeun Lee
Writing – original draft: Yeeun Lee
Writing – review & editing: Myoung-Hwan Ahn, Mina Kang, Dohyeong Kim, Kyung-Jung Moon

et al., 2023) or across a series of satellites, such as the Meteosat or the Geostationary Operational Environmental Satellites (GOES) series (Doelling et al., 2004; Rublev et al., 2018). The characteristic has alternately led to inter-calibration of the GEO sensors through intermediary means such as numerical weather prediction models (Chander et al., 2013; S. J. Lee & Ahn, 2021).

However, there is a unique circumstance where direct GEO-GEO comparison becomes feasible especially when the sub-nadir satellite longitudes of the spacecrafts are exceptionally close. The onboard sensors in this condition observe Earth scenes with coincident optical viewing paths, providing near-perfect angular matching within the entire overlapping domain. GEMS onboard the Geostationary Korea Multi-Purpose Satellite-2B (GK2B) meets this condition through its counterpart, the Advance Meteorological Imager (AMI) onboard its twin satellite, GK2A. The two satellites are positioned within a 0.05° control box centered around 128.2° E longitude. The twin satellite configuration is utilized in various geostationary environmental satellites to be launched soon, including the Meteosat Third Generation (MTG) series. In this context, the results of this study are anticipated to provide a solid foundation for future applications, highlighting the advantages of this approach.

Collocation between twin satellite sensors is very straightforward, producing extensive data sets that cover a full range of signal levels, angle conditions, and wide spatiotemporal areas. This high-quality collocation allows for capturing enough features with minimal noise, forming a useful basis for broadening the understanding of calibration results. These results are presented in Section 3, including the verification of calibration updates (Section 3.1.1), identification of potential dependencies (Section 3.1.2), and temporal investigation (Section 3.2). With these findings, we aim to verify that AMI and GEMS can serve as useful sources for evaluating sensor performance during their operational periods.

2. Data and Methods

2.1. Sensor Specification

2.1.1. GEMS

GEMS scans the Asia-Pacific region (5°S-45°N, 75–145°E) in the east–west direction with a step and dwell mode, while maintaining a fixed north–south field of view of about 7.78° (W. Choi et al., 2019; J. Kim et al., 2020). It is designed to measure spectral radiances ranging from 300 to 500 nm (Level 1B) with a spectral resolution of better than 0.6 nm. Two transmissive solar diffusers and light emitting diode (LED) are deployed as the on-board calibration system. Alongside this system, monitoring and calibration methods have been devised and performed with various statistical approaches since the completion of the in-orbit test in October 2020 (Kang et al., 2020, 2022; Y. Lee et al., 2020).

The assessment has revealed several calibration issues in GEMS solar observations, such as signal dependence along the north–south direction. The dependence is attributed to the unresolved azimuth angle dependence in the bidirectional transmittance distribution function (BTDF) of the solar diffusers (Kang et al., 2023). In this case, the dependence should be shown only in solar irradiance, but not in Earth radiance, due to the shared optical paths within the instrument, except for the solar diffusers. To confirm this, it is necessary to ensure that Earth radiance is free from this dependence. In this situation, inter-calibration with AMI emerges as a useful means to evaluate the issue, given that the collocation data sets can perfectly cancel out scene variabilities.

2.1.2. AMI

AMI has six visible/near infrared and 10 infrared channels for continuous atmospheric monitoring. The first visible channel at a central wavelength of 470 nm ($R_{0.47}$) is employed for the comparison since the spectral response function (SRF) of the channel is fully encompassed by the GEMS observations. To obtain surface information, an infrared channel centered at 10.5 μ m (window channel, $BT_{10.5}$) is collocated together with $R_{0.47}$. This study employs full-disk observations taken at ten-minute intervals for $R_{0.47}$ and $BT_{10.5}$, with spatial resolutions of 1 and 2 km, respectively. For visible and near-infrared channels, the National Meteorological Satellite Center (NMSC) has applied multiple calibration techniques and a quantitative description for the radiometric calibration accuracy is provided in Supporting Information S1 (Text S1 and Table S1). AMI exhibits a systematic bias of approximately 3% (negative) compared to the GSICS reference sensors (LEO), with potential seasonal variations. The calibration results (D. Kim et al., 2021) as well as the related information can be found in the following website (URL: http://210.125.45.71/enhome/html/gsics/vicariousIntroGK2A.do).

19448007, 2024, 14, Downloaded from https://agupubs.onlinelibrary.wiley.com/doi/10.1029/2024GL109364 by Ewha Womans University Library, Wiley Online Library on [30/10/2024]. See the Terms and Conditions (https://onlinelibrary.wiley.com/terms-and-conditions) on Wiley Online Library for rules of use; OA articles are governed by the applicable Creative Commons License

2.2. Ray-Matching

Ray-matching had been developed to relate measured information of GEO and LEO sensors in early days for the Clouds and the Earth's Radiant Energy System (CERES) project (Minnis et al., 1991; Minnis & Harrison, 1984). Afterward, the concept of relating the GEO-LEO measurements has been employed to calibrate GEO imagers by setting a well-calibrated LEO sensor as a reference (Doelling et al., 2016; Minnis et al., 2002a, 2008; Xiong et al., 2020). Targeting specific scenes such as deep convective clouds (DCC) has been further developed as it can reduce the bidirectional reflectance distribution function (BRDF) effects of the clouds (Bhatt et al., 2017; Hu et al., 2004). Setting a particular target contributes to effectively detecting sensor-specific signals, while it reduces the number of data sets as a trade-off. To mitigate this, a statistical approach has been developed especially for the DCC calibration, and it has proven effective in detecting sensor degradation (Doelling et al., 2013).

In this study, we take advantage of ray-matching between AMI and GEMS, all scenes with coinciding optical viewing paths without additional treatment. When empirically checking the position vectors of GK2A and GK2B over the course of a year, the angles between the position vectors in the Earth-centered, Earth-fixed (ECEF) coordinates vary up to 0.06°. This variation introduces viewing angle differences approximately on the order of 0.01–0.1°, which is practically small compared to the current ray-matching condition between GEO-LEO, mostly 1% for the viewing zenith angle (VZA) differences (D. Kim et al., 2021). The advantage guarantees huge collocation data sets, facilitating further data filtering and a more rigorous spatiotemporal match.

2.2.1. Spatial, Temporal, and Spectral Matching

The spatial collocation is performed with a spatial average after re-gridding, to reduce random noises originating from natural scene variability as well as residual uncertainty introduced by data processing such as image navigation and registration (INR) uncertainty. In this study, a grid size of 0.25° is chosen to minimize noise while securing enough collocation data sets, representing valid observational characteristics. A detailed description can be found in Supporting Information S1 (Text S2, Figures S1 and S2, and Table S2). To obtain scene homogeneity information (Doelling et al., 2013), the relative uncertainty (v_i and w_i) given as the ratio between standard deviation and its mean is applied (Hewison, 2013) as follows:

$$v_i = u(X_i)^{-1} = \left(\frac{\sigma(X_i)}{m(X_i)}\right)^{-1} \text{ and } w_i = u(Y_i)^{-1} = \left(\frac{\sigma(Y_i)}{m(Y_i)}\right)^{-1} \quad (1)$$

where σ and m indicates the standard deviation and the mean of reflectances for each grid, respectively. The subscript i indicates the grid index in the collocation data sets and X_i and Y_i are the AMI and GEMS observations within the ith grid. The data sets presented in Section 3.1 particularly undergo screening based on the spatial inhomogeneity condition ($u(X_i)$ <5% and $u(Y_i)$ <5%), since this scene inhomogeneity is closely related to collocation error. It is further employed as weights in the weighted linear regression (refer to Section 2.3).

Temporal matching is performed by calculating the observation time difference for each grid. GEMS provides approximately 700 scan images for 30-min observation. During the GEMS observation, Three or four full-disk images of AMI are taken and pieced together with the temporal match threshold (Δt < 5 min). The temporal matching for a spatially matched grid inherently aligns solar zenith angle (SZA) and solar azimuth angle (SAA) between the sensors without additional treatment.

Finally, hyperspectral radiances of GEMS are convolved with the AMI SRF for spectral matching within the wavelengths of 442–498 nm, following interpolation at spectral intervals of about 0.02 nm. The detailed process for spectral matching is outlined in Supporting Information S1 (Text S3 and Figure S3). The bidirectional reflectance is calculated after the convolution process as follows:

$$R = \frac{\pi I}{\mu_0 F} \quad (2)$$

where F, I, R and μ_0 denotes the measured solar irradiance, Earth radiance, reflectance, and the cosine of SZA for the optical path length correction.

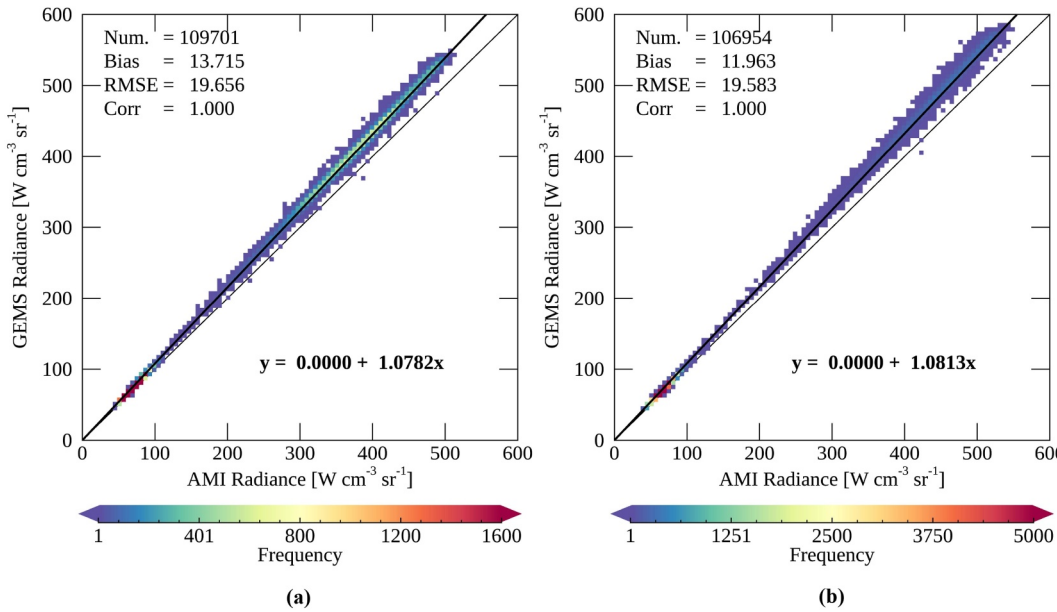


Figure 1. Scatter density plots of AMI and GEMS radiances measured in (a) January and (b) July 2021 (01–06 UTC) with statistics based on the weighted linear regression. The color bar indicates the number of collocation data sets after binning with the bin size of 1 W cm^{-3} sr^{-1}.

2.2.2. Filtering Test

After the collocation process, the grids consisting of land and sun-glint pixels are screened out. Land scenes have higher natural variability increasing variances in radiance biases between AMI and GEMS. Sun-glint scenes corresponding to specular reflection seem to be more sensitive to temporal mismatches, which could add a systematic bias depending on the observation time difference. The SZA and VZA are also limited to 60°, because the grids with larger zenith angles have high collocation error caused by longer optical path lengths (Sterckx et al., 2013). Similarly, longitude is constrained to over 100°E, because the far-western region in the GEMS FOR presents larger variances compared to the nadir positions. The saturation pixels of GEMS are also screened out, of which radiances exceed 592.35 W cm^{-3} sr^{-1} at wavelengths between 450 and 500 nm according to on-ground test results. The number of collocation data sets after these filtering conditions is around 100,000 every month.

2.3. Weighted Linear Regression

To obtain stable signals from the scenes ranging from dark ocean to very bright clouds, we employ weighted linear regression. The relative uncertainty mentioned in Section 2.2.1 serves as a weight for each collocated grid, increasing the contribution from homogeneous scenes. The weighted linear regression slopes become more stable when accounting for the uncertainties associated with X_i and Y_i together. The applied regression method with the weights is the generalized distance regression (GDR) introduced by the following document (ISO/TS 28037, 2010). With further modification, the slopes are further constrained to pass through the origin (0,0) to avoid shifting up and down and ensure stable signals (Kutner et al., 2005).

3. Results and Discussion

AMI and GEMS observations are collected over 2 years from November 2020 to May 2023 every hour during daytime. Figure 1 presents the collocation data sets measured in January and July 2021, showing the regression slopes larger than unity. The positive bias of GEMS is discussed in detail in Section 3.2.1. The correlation presents a good agreement with the coefficients over 0.99 regardless of observation times. With the data sets, the following sections will present spatial and temporal analysis results between AMI and GEMS.

19448007, 2024, 14, Downloaded from https://agupubs.onlinelibrary.wiley.com/doi/10.1029/2024GL109364 by Ewha Womans University Library, Wiley Online Library on [30/10/2024]. See the Terms and Conditions (https://onlinelibrary.wiley.com/terms-and-conditions) on Wiley Online Library for rules of use; OA articles are governed by the applicable Creative Commons License

10.1029/2024GL109364

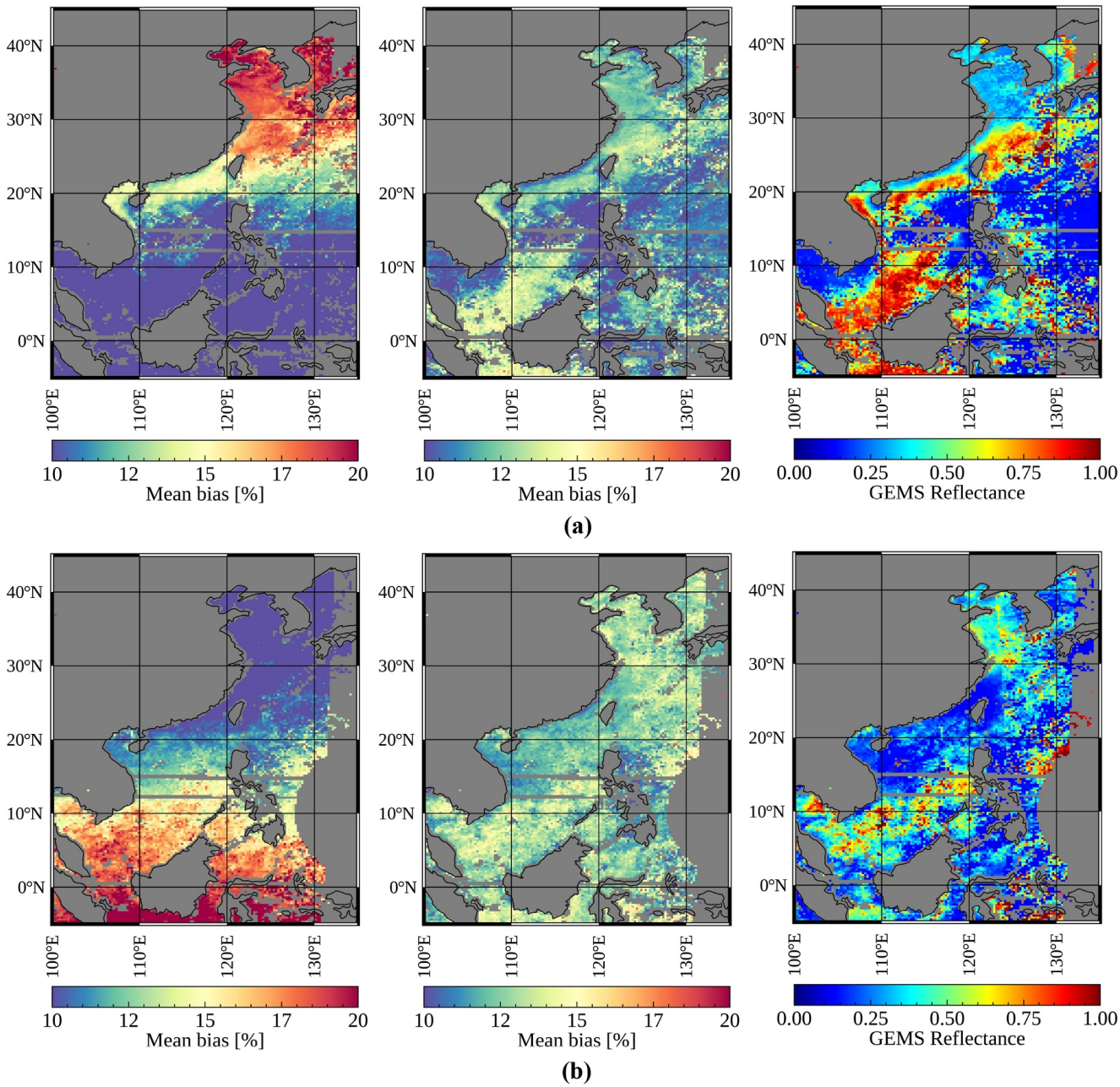


Figure 2. Distribution of mean biases between AMI and GEMS reflectances before (the first column) and after (the second column) the GEMS BTDF update. The third column presents mean reflectances of GEMS for each grid. The collocation data sets are the observations in (a) January and (b) July 2021 (01–06 UTC), and invalid grids including bad pixels (Y. Lee et al., 2023) were filtered out during the collocation process.

3.1. Spatial Analysis

3.1.1. North-South Spatial Dependence

As mentioned earlier, a primary issue regarding GEMS Level 1B products was the north–south spatial dependence in solar irradiance. The dependence is also expected to be present in Earth reflectance (the ratio of Earth radiance to solar irradiance) but not in radiance. To verify this, mean biases of reflectance between AMI and GEMS are calculated with the collocation data sets measured in January and July 2021. As shown in the first column in Figure 2, there is a clear north–south dependence in the mean biases, which is reversed between January and July. On the other hand, the second column in Figure 2 shows consistent biases across all latitudes

19448007, 2024, 14, Downloaded from https://agupubs.onlinelibrary.wiley.com/doi/10.1029/2024GL109364 by Ewha Womans University Library, Wiley Online Library on [30/10/2024]. See the Terms and Conditions (https://onlinelibrary.wiley.com/terms-and-conditions) on Wiley Online Library for rules of use; OA articles are governed by the applicable Creative Commons License

19448007, 2024, 14, Downloaded from https://agupubs.onlinelibrary.wiley.com/doi/10.1029/2024GL109364 by Ewha Womans University Library, Wiley Online Library on [30/10/2024]. See the Terms and Conditions (https://onlinelibrary.wiley.com/terms-and-conditions) on Wiley Online Library for rules of use; OA articles are governed by the applicable Creative Commons License

regardless of seasons, demonstrating the effectiveness of the BTDF update. The improved biases present similar patterns with radiances as presented in Supporting Information S1 (Figure S4). These findings suggest that AMI could be an effective relative standard for evaluating spatial dependence in GEMS, and vice versa.

3.1.2. Signal Dependence

In Figure 2, removing spatial dependence reveals a more pronounced signal dependence. Particularly, positive biases increase more rapidly at lower signals below 0.4, as shown in Figure 3a. The signal dependence is further investigated for darker scenes (AMI $R_{0.47} < 0.3$, $BT_{10.5} > 280$ K, and $u(X_i)$, $u(Y_i) < 1\%$) as a function of SZA and VZA. Figure 3b shows increasing GEMS reflectances with increasing zenith angles due to more scattered light from the ocean surface toward the satellites with high SZA and VZA. The higher zenith conditions result in the increased Rayleigh scattering along the longer optical path and the increased contribution of Fresnel reflection (Fasnacht et al., 2019; Vasilkov et al., 2017). An interesting finding is that reflectance distributions with higher zenith angles exhibit higher mean biases (see Figure 3c), consistent with the results in Figure 3a. This suggests that signal and observation angle dependencies could be intertwined, particularly for lower signals, potentially causing temporal dependence since solar angles vary with time. This indicates that diurnal or seasonal variations may occur due to the sensitivity of reflectance to zenith angles, in addition to atmospheric variations.

3.2. Temporal Analysis

The previous section analyzes dependencies based on geolocation variables, utilizing collocation data sets spanning diverse spatiotemporal conditions. This section focuses on temporal aspects across various observation intervals. For trend monitoring, weighted regression is used leveraging the stable trends exhibited by the indicator.

3.2.1. Radiometric Calibration

Figure 4a presents regression slopes of AMI and GEMS, compared with the GEO-LEO comparison provided by NMSC between AMI and the Visible Infrared Imaging Radiometer Suite (VIIRS) onboard Suomi-NPP and NOAA20. The regression slopes between AMI and GEMS present a more consistent pattern compared to the GEO-LEO ray-matching results, because of stricter collocation thresholds. Nevertheless, the GEO-LEO regression slopes are closer to unity, which confirms that GEMS has a positive bias of approximately 12%–15% in its signals especially beyond 450 nm, demonstrating necessity of an further investigation of its radiometric calibration. Figures 4b and 4c present regression slopes of reflectances and radiances for different scenes, ocean (AMI $R_{0.47} < 0.15$, $BT_{10.5} > 280$ K, and $u(X_i)$, $u(Y_i) < 1\%$), clouds (AMI $R_{0.47} > 0.7$, $BT_{10.5} < 220$ K, and $u(X_i)$, $u(Y_i) < 3\%$) and all targets. Clouds present higher slopes compared to ocean, and the seasonal variations become clearer in reflectances. Regression slopes of radiances are smaller than those of reflectances, presenting that the GEMS solar irradiance may need further correction regarding the systematic bias in irradiance. Most GEMS Level 2 products utilize reflective spectral features for retrieval (J. Kim et al., 2020). While overall systematic bias across spectra may have minimal impact on retrieval under such approaches, it still has the potential to influence specific retrieval processes relying on theoretical irradiance for radiance scaling (Cho et al., 2023) or using an air mass factor (G. Lee et al., 2024).

3.2.2. Diurnal Variation

The GEO-GEO inter-calibration offers unique insights into diurnal variation of measured signals, which are not as readily available through the GEO-LEO comparison. Table 1 presents the statistics of AMI and GEMS radiances measured in 2021 at different observation times (01–06 UTC) with correlation coefficient, regression slope, bias, and root mean square error (RMSE). There is a decreasing trend in both bias and RMSE, which is similarly observed in reflectance across different seasons and surface types (land or ocean). This indicates there is a consistent diurnal influence in the comparison results of AMI and GEMS. Although the cause of this temporal dependence remains unclear, it may stem from various factors, including angle dependence as discussed in Section 3.1.2. Other potential causes include the SRF shift (Text S4, Figure S5, and Table S3 in Supporting Information S1), detector temperature sensitivity (Fangfang et al., 2021), polarization error (H. Choi et al., 2024), or the angle dependence of the scan mirror. In this context, GEO-GEO inter-calibration stands out as an effective

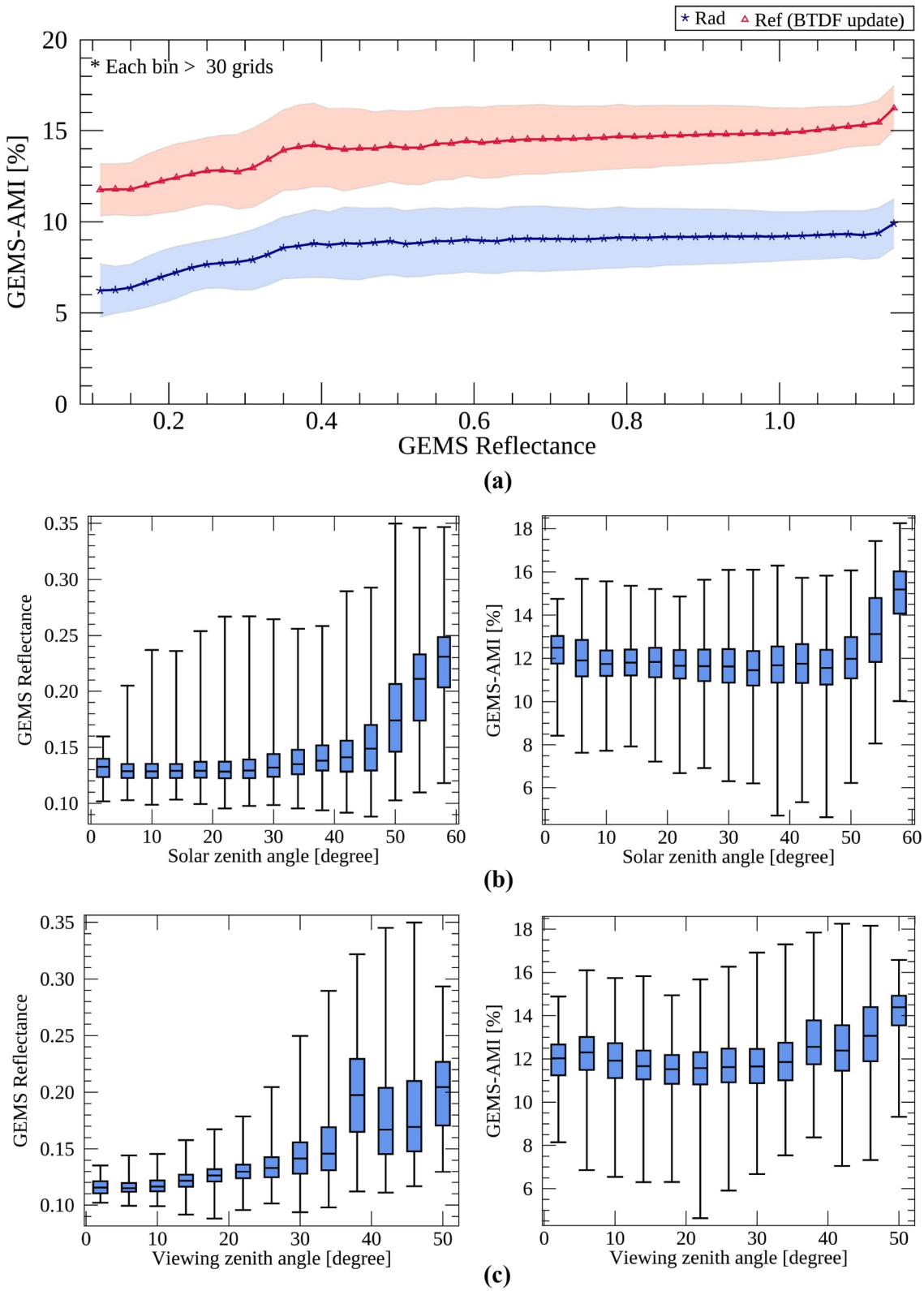


Figure 3. Signal dependence in (a) mean biases of radiances (blue asterisks) and reflectances (red triangles) between AMI and GEMS, grouped by the GEMS reflectances with a class width of 0.02. The second and third rows present box plots for darker scenes (AMI $R_{0.47} < 0.3$, AMI $BT_{10.5} > 280$ K, and $u(X_i)$, $u(Y_i) < 1\%$) showing (b) SZA and (c) VZA dependences for GEMS reflectances and the biases with a class width of 4°.

19448007, 2024, 14, Downloaded from https://agupubs.onlinelibrary.wiley.com/doi/10.1029/2024GL109364 by Ewha Womans University Library, Wiley Online Library on [30/10/2024]. See the Terms and Conditions (https://onlinelibrary.wiley.com/terms-and-conditions) on Wiley Online Library for rules of use; OA articles are governed by the applicable Creative Commons License

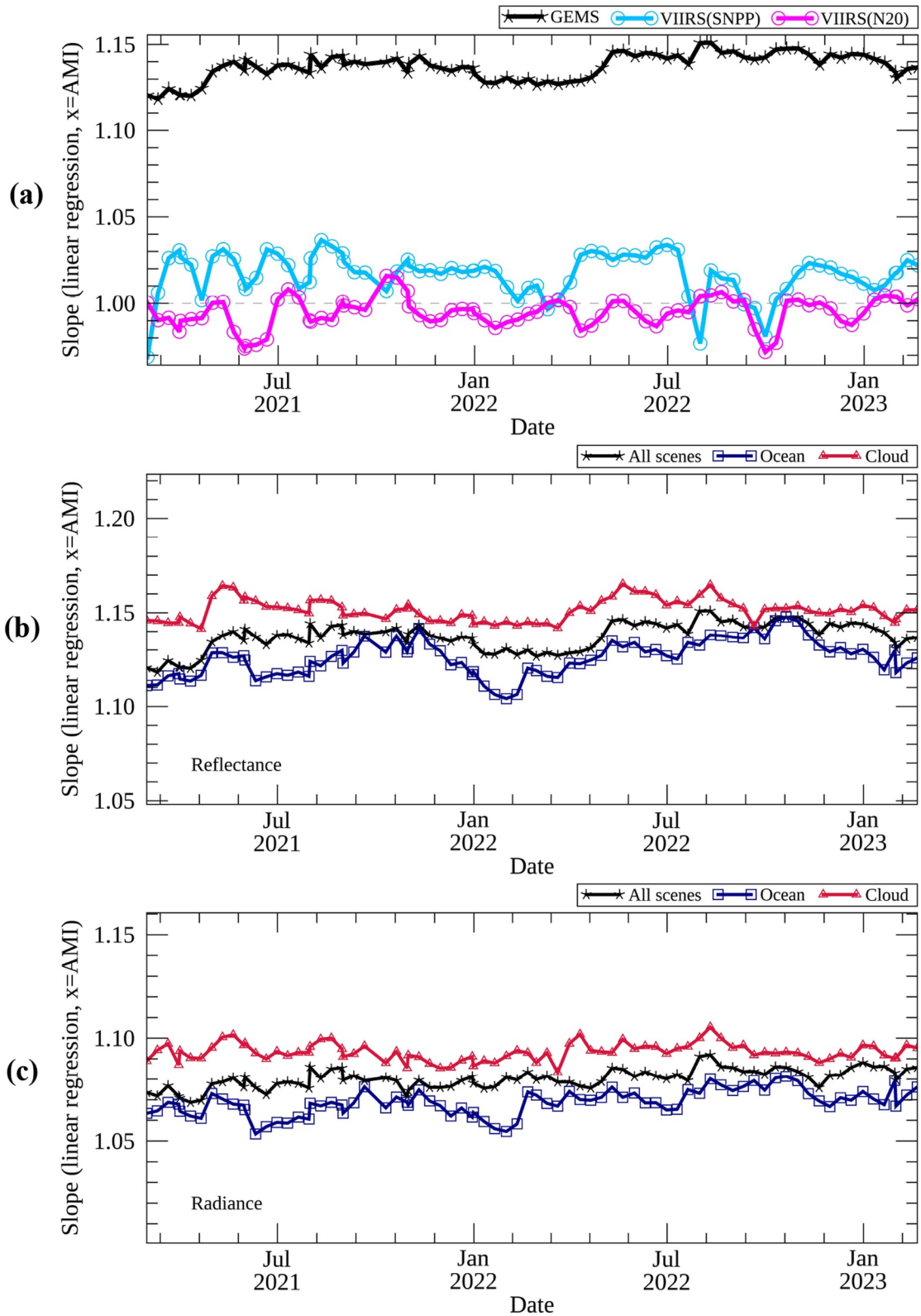


Figure 4. Regression slopes of (a) reflectances derived from AMI with GEMS (black triangles) and VIIRS onboard Suomi-NPP and NOAA-20 (blue and magenta circles, respectively). Panel (b) displays regression slopes of reflectances for all scenes (black asterisks), ocean (blue squares), and clouds (red triangles). The data is collected from March 2021 to February 2023, presented using a 10-day running mean.

19448007, 2024, 14, Downloaded from https://agupubs.onlinelibrary.wiley.com/doi/10.1029/2024GL109364 by Ewha Womans University Library, Wiley Online Library on [30/10/2024]. See the Terms and Conditions (https://onlinelibrary.wiley.com/terms-and-conditions) on Wiley Online Library for rules of use; OA articles are governed by the applicable Creative Commons License

19448007, 2024, 14, Downloaded from https://agupubs.onlinelibrary.wiley.com/doi/10.1029/2024GL109364 by Ewha Womans University Library, Wiley Online Library on [30/10/2024]. See the Terms and Conditions (https://onlinelibrary.wiley.com/terms-and-conditions) on Wiley Online Library for rules of use; OA articles are governed by the applicable Creative Commons License

Table 1
Statistics of AMI and GEMS Radiances Measured in 2021 at Different Observation Times Ranging From 1 to 6 UTC

UTC	Correlation coefficient	Slope	Bias [W cm^{-3} sr^{-1}]	RMSE [W cm^{-3} sr^{-1}]
1 (10 KST)	1.00	1.083	10.7	17.4
2 (11 KST)	1.00	1.078	10.1	16.2
3 (12 KST)	1.00	1.077	9.7	15.6
4 (13 KST)	1.00	1.077	10.1	16.3
5 (14 KST)	1.00	1.078	9.7	15.6
6 (15 KST)	1.00	1.081	7.8	12.9

tool, leveraging vast data sets to evaluate the influence of these factors and their potential updates. Considering this, the results emphasize the potential of the GEO-GEO inter-calibration in enhancing our understanding of temporal fluctuations, thereby possibly refining inter-calibration methodologies in future research.

4. Conclusions

This research introduces an inter-calibration method, specifically utilizing ray-matching, to compare and monitor Level 1B products between instruments onboard twin satellites, GEMS/GK2B and AMI/GK2A. The close alignment of their sub-nadir positions offers a practical advantage, enabling matched optical viewing paths and generating extensive collocation data sets that cover a broad range of observation conditions.

With the data sets over 2 years, we conduct comprehensive spatial and temporal analyses between AMI and GEMS. The spatial analysis successfully addresses the calibration update of GEMS for solar irradiance and reflectance, though signal and angle dependencies underscore the need for further investigation. Temporal analysis reveals sensor drifts and radiometric uncertainties in GEMS radiances of about 4%–7%, considering the AMI radiometric accuracy. The GEO-GEO inter-calibration verifies diurnal variations in measured signals, which are less apparent in GEO-LEO comparisons. The results highlight its potential as an effective means for identifying an issue and evaluating its update on the radiance level.

Our findings present the critical role of GEO-GEO inter-calibration in enhancing our understanding of the measurement characteristics. Future investigations should focus on identifying the root causes of observed dependencies and biases, thereby advancing the effectiveness of inter-calibration techniques. This study aims to inform and facilitate future research endeavors, potentially aiding in the monitoring of sensors in similar configurations.

Data Availability Statement

The AMI Level 1B products are available at https://datasvc.nmsc.kma.go.kr/datasvc/html/main/main.do?lang=en (NMSC, 2019). The AMI SRFs for all channels and land sea mask are also available at https://datasvc.nmsc.kma.go.kr/datasvc/html/base/cmm/selectPage.do?page=static.software (NMSC, 2019). The GSICS inter-calibration coefficients between AMI and VIIRS were provided by NMSC, and the coefficients can be reproduced by applying the methodology described in D. Kim et al. (2021). The GEMS Level 1C products can be accessed through the SFTP service provided by the Environmental Satellite Center (ESC) of the National Institute of Environmental Research (NIER) (https://nesc.nier.go.kr/en/html/cntnts/91/static/page.do), following approval from the institute (ESC, 2020). The data sets are not publicly available so far due to the regulation of the institution for the Level 1C products, and the data sets are accessible to researchers only volunteering on the GEMS calibration and validation project. The MATLAB code for the weighted regression algorithm is freely available at https://www.npl.co.uk/resources/software/iso-ts-28037-2010e (NPL, 2014).

Acknowledgments
This research has been supported by the Basic Science Research Program through the National Research Foundation of Korea (NRF) funded by the Ministry of Education (Grant Number 2018R1A6A1A08025520). The two anonymous reviewers are greatly appreciated for their constructive and careful comments on the manuscript.

References

Bhatt, R., Doelling, D., Scarino, B., Haney, C., & Gopalan, A. (2017). Development of seasonal BRDF models to extend the use of deep convective clouds as invariant targets for satellite SWIR-band calibration. *Remote Sensing*, *9*(10), 1061. https://doi.org/10.3390/rs9101061

Chander, G., Hewison, T. J., Fox, N., Wu, X., Xiong, X., & Blackwell, W. J. (2013). Overview of intercalibration of satellite instruments. *IEEE Transactions on Geoscience and Remote Sensing*, *51*(3), 1056–1080. https://doi.org/10.1109/TGRS.2012.2228654

Cho, Y., Kim, J., Go, S., Kim, M., Lee, S., Kim, M., et al. (2023). First atmospheric aerosol monitoring results from geostationary environment monitoring spectrometer (GEMS) over Asia. *Atmospheric Measurement Techniques Discussions*, *2023*, 1–29. https://doi.org/10.5194/amt-2023-221

Choi, H., Liu, X., Jeong, U., Chong, H., Kim, J., Ahn, M. H., et al. (2024). Geostationary environment monitoring spectrometer (GEMS) polarization characteristics and correction algorithm. *Atmospheric Measurement Techniques*, *17*(1), 145–164. https://doi.org/10.5194/AMT-17-145-2024

Choi, W., Moon, K.-J., Yoon, J., Cho, A., Kim, S., Lee, S., et al. (2019). Introducing the geostationary environment monitoring spectrometer. *Journal of Applied Remote Sensing*, *13*(01), 1. https://doi.org/10.1117/1.jrs.13.019901

Di, D., Liu, Y., Li, J., Zhou, R., Li, Z., & Gong, X. (2023). Inter-calibration of geostationary imager infrared bands using a hyperspectral sounder on the same platform. *Geophysical Research Letters*, *50*(3), e2022GL101628. https://doi.org/10.1029/2022GL101628

Doelling, D. R., Haney, C. O., Scarino, B. R., Gopalan, A., & Bhatt, R. (2016). Improvements to the geostationary visible imager ray-matching calibration algorithm for CERES edition 4. *Journal of Atmospheric and Oceanic Technology*, *33*(12), 2679–2698. https://doi.org/10.1175/JTECH-D-16-0113.1

Doelling, D. R., Morstad, D., Scarino, B. R., Bhatt, R., & Gopalan, A. (2013). The characterization of deep convective clouds as an invariant calibration target and as a visible calibration technique. *IEEE Transactions on Geoscience and Remote Sensing*, *51*(3), 1147–1159. https://doi.org/10.1109/TGRS.2012.2225066

Doelling, D. R., Nguyen, L., & Minnis, P. (2004). Calibration comparisons between SEVIRI, MODIS and GOES data. In H. Lacoste (Ed.), *Proceedings of the second MSG RAO workshop* (pp. 149–153). Salzburg.

Environmental Satellite Center of Environmental Research. (2020). GEMS level 1C products [Dataset]. *ESC NIER SFTP Service*. https://nesc.nier.go.kr/en/html/cntnts/91/static/page.do

Fangfang, Y., Xiangqian, W., Haifeng, Q., & Jon, F. (2021). Calibration anomaly for GOES-17 ABI infrared images before local midnight [PowerPoint Slides]. *CALCON Technical Meeting*. https://digitalcommons.usu.edu/calcon/CALCON2021/all2021content/2/

Fasnacht, Z., Vasilkov, A., Haffner, D., Qin, W., Joiner, J., Krotkov, N., et al. (2019). A geometry-dependent surface Lambertian-equivalent reflectivity product for UV–Vis retrievals – Part 2: Evaluation over open Ocean. *Atmospheric Measurement Techniques*, *12*(12), 6749–6769. https://doi.org/10.5194/amt-12-6749-2019

Hewison, T. J. (2013). An evaluation of the uncertainty of the GSICS SEVIRI-IASI intercalibration products. *IEEE Transactions on Geoscience and Remote Sensing*, *51*(3), 1171–1181. https://doi.org/10.1109/TGRS.2012.2236330

Hu, Y., Wielicki, B. A., Yang, P., Stackhouse, P. W., Lin, B., & Young, D. F. (2004). Application of deep convective cloud albedo observation to satellite-based study of the terrestrial atmosphere: Monitoring the stability of spaceborne measurements and assessing absorption anomaly. *IEEE Transactions on Geoscience and Remote Sensing*, *42*(11), 2594–2599. https://doi.org/10.1109/TGRS.2004.834765

International Organization for Standardization Technical Specification (ISO/TS). (2010). *ISO 28037:2010 determination and use of straight-line calibration functions*. International Organization for Standardization (ISO). Retrieved from https://www.iso.org/standard/44473.html

Jiang, G.-M., Yan, H., & Ma, L.-L. (2009). Intercalibration of SVISSR/FY-2C infrared channels against MODIS/Terra and AIRS/Aqua channels; intercalibration of SVISSR/FY-2C infrared channels against MODIS/Terra and AIRS/Aqua channels. *IEEE Transactions on Geoscience and Remote Sensing*, *47*(5), 1548–1558. https://doi.org/10.1109/TGRS.2008.2005200

Kang, M., Ahn, M. H., Ko, D. H., Kim, J., Nicks, D., Eo, M., et al. (2022). Characteristics of the spectral response function of geostationary environment monitoring spectrometer analyzed by ground and in-orbit measurements. *IEEE Transactions on Geoscience and Remote Sensing*, *60*, 1–16. https://doi.org/10.1109/TGRS.2021.3091677

Kang, M., Ahn, M.-H., Lee, Y., Eo, M., & Kim, J. (2023). GEMS performance and lessons learned [PowerPoint slides]. *Committee on Earth Observation Satellites (CEOS) AC-VC-19/ACSG Joint Meeting*. https://ceos.org/document_management/Virtual_Constellations/AC-VC/Meetings/AC-VC-19/presentations/Presentations%20PDF/2.%20Wed%2025%20Oct%202023%20-%20TRACE%20GASES%20AND%20AEROSOLS%20AIR%20QUALITY/We-14_Kang_GEMS_v1.pdf

Kang, M., Ahn, M. H., Liu, X., Jeong, U., & Kim, J. (2020). Spectral calibration algorithm for the geostationary environment monitoring spectrometer (Gems). *Remote Sensing*, *12*(17), 1–17. https://doi.org/10.3390/rs12172846

Kim, D., Gu, M., Oh, T.-H., Kim, E.-K., & Yang, H.-J. (2021). Introduction of the advanced meteorological imager of Geo-Kompsat-2a: In-orbit tests and performance validation. *Remote Sensing*, *13*(7), 1303. https://doi.org/10.3390/rs13071303

Kim, J., Jeong, U., Ahn, M. H., Kim, J. H., Park, R. J., Lee, H., et al. (2020). New era of air quality monitoring from space: Geostationary environment monitoring spectrometer (GEMS). *Bulletin of the American Meteorological Society*, *101*(1), E1–E22. https://doi.org/10.1175/BAMS-D-18-0013.1

Kutner, M. H., Nachtsheim, C. J., Neter, J., & Li, W. (2005). *Applied linear statistical models (Fifth edition)*. McGraw-Hill.

Lee, G. T., Park, R. J., Kwon, H.-A., Ha, E. S., Lee, S. D., Shin, S., et al. (2024). First evaluation of the GEMS formaldehyde product against TROPOMI and ground-based column measurements during the in-orbit test period. *Atmospheric Chemistry and Physics*, *24*(8), 4733–4749. https://doi.org/10.5194/acp-24-4733-2024

Lee, S. J., & Ahn, M.-H. (2021). Synergistic benefits of intercomparison between simulated and measured radiances of imagers onboard geostationary satellites. *IEEE Transactions on Geoscience and Remote Sensing*, *59*(12), 10725–10737. https://doi.org/10.1109/TGRS.2021.3054030

Lee, Y., Ahn, M. H., & Kang, M. (2020). The new potential of deep convective clouds as a calibration target for a geostationary UV/VIS hyperspectral spectrometer. *Remote Sensing*, *12*(3), 446. https://doi.org/10.3390/rs12030446

Lee, Y., Ahn, M.-H., Kang, M., & Eo, M. (2023). Spectral replacement using machine learning methods for continuous mapping of the geostationary environment monitoring spectrometer (GEMS). *Atmospheric Measurement Techniques*, *16*(1), 153–168. https://doi.org/10.5194/AMT-16-153-2023

Minnis, P., Doelling, D. R., Nguyen, L., Miller, W. F., & Chakrapani, V. (2008). Assessment of the visible channel calibrations of the VIRS on TRMM and MODIS on Aqua and Terra. *Journal of Atmospheric and Oceanic Technology*, *25*(3), 385–400. https://doi.org/10.1175/2007JTECHA1021.1

Minnis, P., & Harrison, E. F. (1984). Diurnal variability of regional cloud and clear-sky radiative parameters derived from GOES data. Part III: November 1978 radiative parameters. *Journal of Applied Meteorology and Climatology*, *23*(7), 1032–1051. https://doi.org/10.1175/1520-0450(1984)023

Minnis, P., Nguyen, L., Doelling, D. R., Young, D. F., Miller, W. F., & Kratz, D. P. (2002a). Rapid calibration of operational and research meteorological satellite imagers. Part I: Evaluation of research satellite visible channels as references. *Journal of Atmospheric and Oceanic Technology*, *19*(9), 1233–1249. https://doi.org/10.1175/1520-0426(2002)019<1233:RCOOAR>2.0.CO;2

19448007, 2024, 14, Downloaded from https://agupubs.onlinelibrary.wiley.com/doi/10.1029/2024GL109364 by Ewha Womans University Library, Wiley Online Library on [30/10/2024]. See the Terms and Conditions (https://onlinelibrary.wiley.com/terms-and-conditions) on Wiley Online Library for rules of use; OA articles are governed by the applicable Creative Commons License

Minnis, P., Nguyen, L., Doelling, D. R., Young, D. F., Miller, W. F., & Kratz, D. P. (2002b). Rapid calibration of operational and research meteorological satellite imagers. Part II: Comparison of infrared channels. *Journal of Atmospheric and Oceanic Technology*, *19*(9), 1250–1266. https://doi.org/10.1175/1520-0426(2002)019<1250:RCOOAR>2.0.CO;2

Minnis, P., Young, D. F., & Harrison, E. F. (1991). Examination of the relationship between outgoing infrared window and total Longwave fluxes using satellite data. *Journal of Climate*, *4*(11), 1114–1133. https://doi.org/10.1175/1520-0442(1991)004<1114:EOTRBO>2.0.CO;2

National Meteorological Satellite Center. (2019a). AMI level 1B products [Dataset]. *NMSC Data Service* https://datasvc.nmsc.kma.go.kr/datasvc/html/main/main.do?lang=en

National Meteorological Satellite Center. (2019b). AMI spectral response functions and land sea masks [Dataset]. *NMSC Data Service*. https://datasvc.nmsc.kma.go.kr/datasvc/html/base/cmm/selectPage.do?page=static.software

National Physical Laboratory. (2014). Determination and use of straight-line calibration functions [Software]. *NPL Resources*. https://www.npl.co.uk/resources/software/iso-ts-28037-2010e

Rublev, A. N., Gorbarenko, E. V., Golomolzin, V. V., Borisov, E. Y., Kiseleva, J. V., Gektin, Y. M., & Zaitsev, A. A. (2018). Inter-calibration of infrared channels of geostationary meteorological satellite imagers. *Frontiers in Environmental Science*, *6*(NOV), 410267. https://doi.org/10.3389/FENVS.2018.00142/BIBTEX

Sterckx, S., Livens, S., & Adriaensen, S. (2013). Rayleigh, deep convective clouds, and cross-sensor desert vicarious calibration validation for the PROBA-V mission. *IEEE Transactions on Geoscience and Remote Sensing*, *51*(3), 1437–1452. https://doi.org/10.1109/TGRS.2012.2236682

Vasilkov, A., Qin, W., Krotkov, N., Lamsal, L., Spurr, R., Haffner, D., et al. (2017). Accounting for the effects of surface BRDF on satellite cloud and trace-gas retrievals: A new approach based on geometry-dependent lambertian equivalent reflectivity applied to OMI algorithms. *Atmospheric Measurement Techniques*, *10*(1), 333–349. https://doi.org/10.5194/amt-10-333-2017

Xiong, X., Angal, A., Chang, T., Chiang, K., Lei, N., Li, Y., et al. (2020). MODIS and VIIRS calibration and characterization in support of producing long-term high-quality data products. *Remote Sensing 2020*, *12*(19), 3167. https://doi.org/10.3390/RS12193167

Zoogman, P., Liu, X., Suleiman, R. M., Pennington, W. F., Flittner, D. E., Al-Saadi, J. A., et al. (2017). Tropospheric emissions: Monitoring of pollution (TEMPO). *Journal of Quantitative Spectroscopy and Radiative Transfer*, *186*, 17–39. https://doi.org/10.1016/j.jqsrt.2016.05.008

References From the Supporting Information

Lee, H. (2024). KMA GDWD activities 2024 [PowerPoint slides]. *GSICS Annual Meeting 2024*. http://gsics.atmos.umd.edu/pub/Development/AnnualMeeting2024/3l_GDWG_2024_KMA_Hanbyul%20Lee_final.pptx

Lyapustin, A., Wang, Y., Choi, M., Xiong, X., Angal, A., Wu, A., et al. (2023). Calibration of the SNPP and NOAA 20 VIIRS sensors for continuity of the MODIS climate data records. *Remote Sensing of Environment*, *295*, 113717. https://doi.org/10.1016/J.RSE.2023.113717

19448007, 2024, 14, Downloaded from https://agupubs.onlinelibrary.wiley.com/doi/10.1029/2024GL109364 by Ewha Womans University Library, Wiley Online Library on [30/10/2024]. See the Terms and Conditions (https://onlinelibrary.wiley.com/terms-and-conditions) on Wiley Online Library for rules of use; OA articles are governed by the applicable Creative Commons License